SAND2013-8720C

IN-SITU MONITORING OF VANADIUM DIOXIDE FORMATION USING HIGH TEMPERATURE XRD

Mark A. Rodriguez, Nelson S. Bell, James J. M. Griego,
Cynthia V. Edney, and Paul G. Clem

Sandia National Laboratories, Albuquerque, NM 87185-1411

ABSTRACT

The monoclinic to tetragonal phase transition (~70°C) in vanadium dioxide (VO_2) strongly impacts the IR properties of the VO_2 compound, which enables its use in applications such as smart window devices. Synthesis of VO_2 can be challenging due to the variability of vanadium oxide phases that may be formed. We have employed High Temperature X-Ray Diffraction (HTXRD) to monitor the reaction process of Vanadium Oxide Precursor (VOP) powders to form the desired tetragonal VO_2 phase. Single phase tetragonal VO_2 was formed within 30 minutes at 420°C in flowing N_2 gas (~50 ppm O_2). The monoclinic-to-tetragonal phase transformation was observed via HTXRD at ~70°C with the typical ~10°C hysteresis (i.e. approached from above or below the transition).

INTRODUCTION

Due to vanadium's variable oxidation state, many different phases of vanadium oxide exist. In addition to stoichiometric variation, different polymorphs for the same chemical formula are observed, further extending the possible phases of vanadium oxide. Such a rich variety of stoichiometries and structures ultimately has an impact on the observed properties and performance of these materials. For the vanadium oxide point-compound having the chemical formula VO_2, Metal-Insulator Transition (MIT) type behavior has been observed. These so-called MIT materials display radical changes in electrical and optical properties as a result of a structural phase transition. For example, a phase transformation (monoclinic to tetragonal) in VO_2 at ~70°C displays a 10^4 to 10^5 magnitude increase in electrical conductivity (Lu, *et al.*, 2011). Concurrent with the change in electrical conductivity is a corresponding change in optical properties (Yang, *et al.*, 2011). In particular, the monoclinic VO_2 phase displays good optical transmission in the visible and near infrared (IR) ranges. In contrast, the tetragonal form (above ~70°C), shows a very sharp decrease in the IR transmittance. These dramatic and reversible property changes can be tailored into engineering applications such as optical switches (Briggs, *et al.*, 2010), sensors (Yang, *et al.*, 2011), and window coatings (Manning, *et al.*, 2004). Figure 1 shows the crystal structures of the VO_2 MIT-paired phases. At room temperature, VO_2 displays a monoclinic structure (Longo & Kierkegaard; 1970) as shown on the left side of Figure 1. This monoclinic phase, hereafter referred to as VO_2 (M), is characterized by alternating V-V distances within the lattice; the structure shows a short V-V distance (2.62 Å) and a relatively long V-V distance (3.17 Å). The differing V-V bond lengths affect the electronic band structure,

resulting in semiconducting behavior for the VO_2 (M) compound (Lu, *et al*., 2011; Lazarovits, *et al.*, 2010). In contrast, the tetragonal form of VO_2, shown in Figure 1 (right), has a more simplified Rutile-type structure (Rogers, 1993) and uniform V-V bond distances (2.87 Å). This tetragonal VO_2, hereafter referred to as VO_2 (T), displays low electrical resistivity as well as a decrease in transmission of the near-IR wavelengths (Lu, *et al.*, 2011).

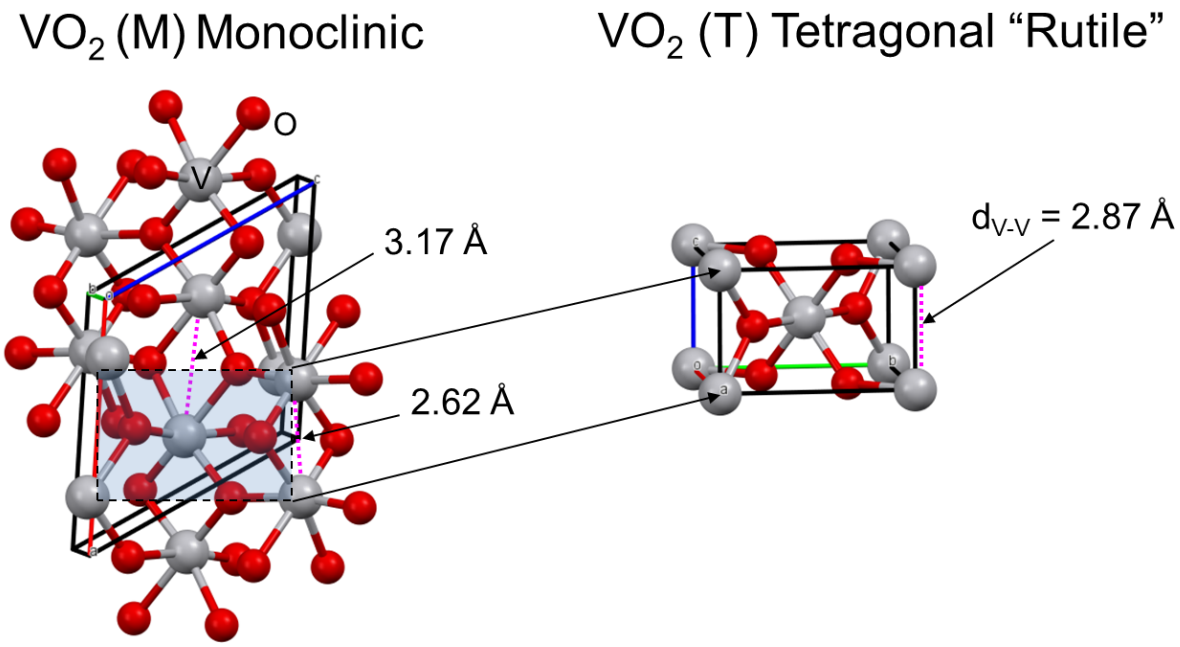

Figure 1. Monoclinic VO_2 (left) showing two distinct V-V bond distances, and tetragonal VO_2 (right) displaying the Rutile-like structure and single V-V distance. See text for details.

The suppression of IR transmission with temperature makes VO_2 an interesting material for smart window applications. Manning, *et al.*, (2004) showed that tungsten-doped VO_2 window coatings could suppress IR transmission at temperatures above the MIT transition. Of late, there has been interest in the synthesis of VO_2 nanoparticles (Yamamoto, *et al.*, 2009; Lu, *et al.*, 2011) for fabrication of low-cost coatings for windows to passively reduce heat transmission. While nanoparticle synthesis has been successful, the demands concerning control of temperature and partial pressure of oxygen (pO_2) during synthesis are evident in some of the more elaborate processing protocols. For example, the route described by Lu, *et al.*, (2011) involves heat treatment of chemically prepared vanadium oxide precursor powder to 300°C in air to form V_2O_5, with subsequent reduction in H_2 at 400°C (forming V_2O_3) followed by an anneal in N_2 gas at 400°C to form the desired VO_2 composition. The focus of our research effort regarding VO_2 material synthesis has been to reduce the complexity of the processing protocols to a single processing schedule through the use of in-situ High Temperature X-ray Diffraction (HTXRD) characterization. This technique ensures that the correct conditions for VO_2 (T) stability and single-phase-formation may be established. This understanding greatly reduces the complexity (and cost) of material synthesis. Herein we describe the use of HTXRD to monitor the various phases that can form under differing time-temperature-pO_2 conditions. To facilitate this discussion, Table 1 gives a summary of all the vanadium oxide phases observed in this

manuscript, their corresponding Powder Diffraction File (PDF) entries (ICDD, 2012), and their structural references. In this way, there shall be no ambiguity regarding the compounds discussed.

Table 1. Vanadium oxide phases observed and discussed within this manuscript.

Phase	PDF entry	Reference
V_2O_3	04-004-2833	Vincent, *et al.,* (1980)
VO_2 (M)	00-043-1051	Longo & Kierkegaard (1970)
VO_2 (B)	04-007-0514	Oka, *et al.,* (1993)
VO_2 (T)	01-079-1655	Rogers (1993)
V_6O_{13}	04-007-1362	Wilhelmi, *et al.,* (1971)
V_3O_7	04-007-0598	Waltersson, *et al.,* (1974)
V_2O_5	00-041-1426	Enjalbert & Galy (1986)

EXPERIMENTAL

Vanadium Oxide Precursor (VOP) Synthesis

Vanadium (V) triethoxide (95%; Aldrich), anhydrous pyridine (99.8%; Sigma-Aldrich) and acetone (99.8%, extra dry; Acros) were all used as received. Deionized water was purified using a Millipore Synergy 185 system to 18.2 MΩ resistance. The precipitation procedure for monodisperse Vanadium Oxide Precursor (VOP) particles was taken from Yamamoto, *et al.* (2009) and conducted within an Argon glove box. Pyridine (13 ml) was measured into a beaker, and 185 μl of Vanadium(V) isopropoxide was added to create a yellow, transparent solution. A second beaker was used to mix 24 ml of acetone with 30 μl of water. A magnetic stir-bar was used for mixing in the acetone-water solution as the pyridine-vanadium solution was added by rapid pouring. An opaque, orange precipitate formed immediately. The solution was allowed to stir for 30 minutes, after which it was transferred to a polyethylene centrifugation tube, and removed from the glovebox. The precipitate was recovered and washed using three cycles of centrifugation and redispersion using pure acetone. The final VOP powder was allowed to air dry overnight in a drying oven set to 90 °C. Scanning Electron Microscopy (SEM) of the VOP powder was performed using a Carl Zeiss Supra™ 55VP SEM (10 to 20kV; 8.5 mm working distance). SEM images were employed to assess the morphology of the generated VOP precursor. Figure 2(a) shows an image of the dried VOP particles illustrating the anticipated spherical morphology and submicron dimensionality. Preliminary XRD analysis of the room temperature VOP material (prior to in-situ heat treatment) confirmed the observation of a broad diffraction peak at ~8.3^o 2θ, characteristic of the nanocrystalline VOP material (Yamamoto, *et al.* 2009); see Figure 2(b). This material was used in subsequent in-situ high-temperature XRD analysis. It is worth noting here that timely harvesting and drying of the VOP precipitate (i.e. < 3 hrs after precipitate formation) was necessary to assure the spherical shape of the nanocrystallite particles and observe the broad 8.3^o 2θ peak in the initial XRD pattern. If harvesting was postposed, recrystallization of VOP material occurred and the spherical morphology was lost in favor of larger single crystals (> 1 μm) with a bladed morphology.

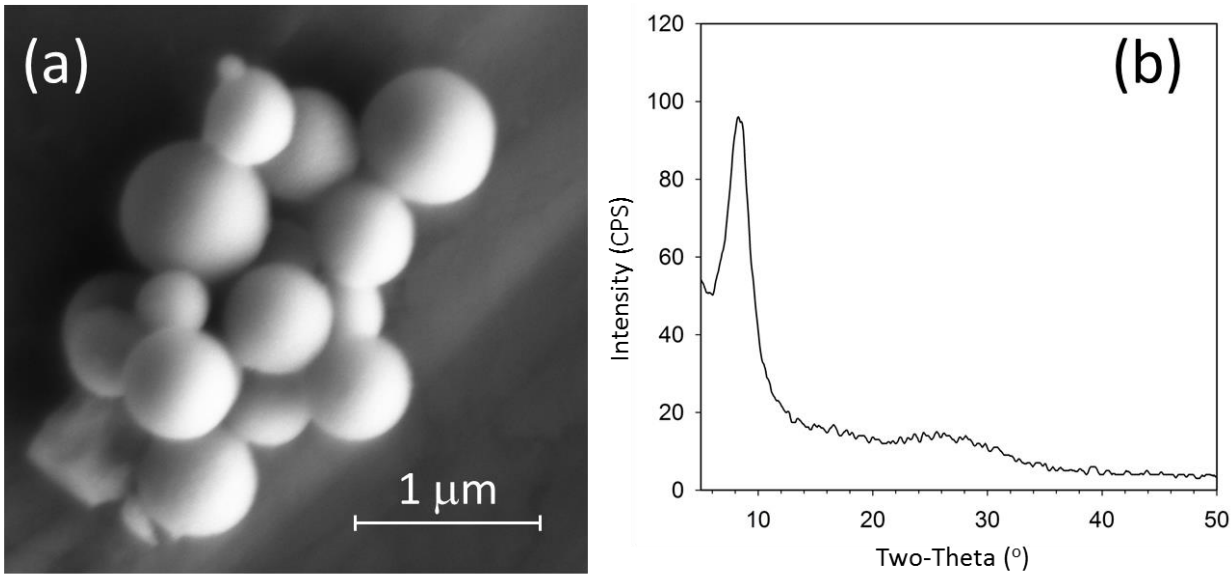

Figure 2. Characterization of Vanadium Oxide Precursor (VOP) powder. (a) SEM image of dried VOP powder showing spherical morphology. (b) XRD pattern showing broad, low-angle peak (~8.3° 2θ) characteristic of VOP precursor.

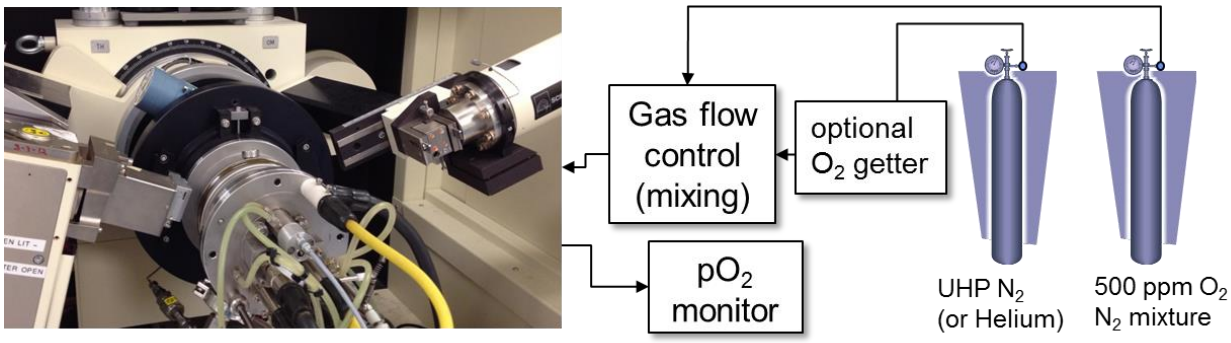

Figure 3. High Temperature XRD setup for in-situ XRD analysis.

High Temperature X-ray Diffraction

High temperature XRD experiments were performed using a Scintag PAD X θ–θ diffractometer (Thermo Electron Inc.; Waltham, MA). This diffractometer was equipped with a sealed-tube source (Cu K_α radiation), an incident-beam mirror optic, a Peltier-cooled Ge solid-state detector, and a Buehler hot-stage with Pt/Rh heating strip and surround heater. X-ray generator settings were 40 kV and 30 mA, and fixed slits were employed. Temperature calibration was performed using thermal expansion behavior of know materials (e.g. alumina) and calibrated to ±5 °C. The heating chamber was configured to handle mixed gas atmospheres, for example: inert (Helium),

N_2, air, and N_2/O_2 mixtures. The He (inert) gas was run through an oxygen getter to reduce the pO_2 to below 1 ppm. An oxygen monitor was placed on the downstream side of the chamber to monitor pO_2 during the experiments, and the pO_2 values were calibrated using certified N_2/O_2 gas mixtures. Figure 3 shows a photo of the Buehler hot stage mounted on the diffractometer as well as a schematic of the gas handling system that was used. To prepare a sample for HTXRD, the dried VOP powder was dispersed in methanol and a dropper was used to deposit this slurry as a thin layer onto 1 cm^2 Si single-crystal substrates. Once the sample was dry, it was placed directly on the hot stage. Samples were typically heated using a 20°C/min ramp rate to the desired analysis temperature. Diffraction patterns were collected over a scan range of 20-80° 2θ at a step-size of 0.04° 2θ and a count time of 1 second. Typical scans were collected in ~30 minute increments.

RESULTS AND DISCUSSION

Determination of the proper conditions for synthesis of VO_2 (T) was an iterative process. Many experiments were performed to map out the reaction progression, determine observed phases, and ultimately fine-tune the time-temperature-pO_2 conditions to obtain phase pure VO_2 (T) at temperature. The VOP precursor material had a spherical morphology after initial synthesis as illustrated in Figure 2(a). For potential applications of the VO_2 material, it was desirable to maintain, as much as possible, the spherical and submicron nature of the VOP particle morphology. Obtaining full conversion to VO_2 (T) while simultaneously preventing particle sintering was paramount for the processing protocol, and it was desired that this occur at the lowest temperature and shortest time possible. Typical in-situ HTXRD measurements involved a fixed pO_2 setting with XRD scans occurring over a set of steps in temperature (e.g. 100, 120, 140°C, etc.). Typically, the temperature steps were in 20°C increments. This type of experiment will hereafter be referred to as a "step-series." The first step-series experiment was performed under gettered Helium (inert) gas with a pO_2 of <1 ppm. The result (not shown) was the formation of V_2O_3 at ~450°C. The V_2O_3 phase persisted up to 600°C and higher. A second step-series was performed in air and showed formation of V_2O_5 as low as ~240°C. This V_2O_5 phase remained present over all measured temperatures up to melting (~680°C). These two measurements bracketed the extremes of the processing and indicated that adjustment in pO_2 should allow isolation of the correct VO_2 stoichiometry.

Figure 4 shows the results of the step-series for pO_2 of ~500 ppm O_2. This plot shows XRD scans as a rainbow color contour plot where low counts are purple and blue, while higher intensity are shown as yellow and red. Temperature increases as one steps from the bottom to the top of the figure. This result illustrates the plethora of phases that occur during heating of the VOP material in this pO_2 range. One quickly notes that below 100°C one can still detect the broad VOP "precursor" peak at ~8.3° 2θ similar to that observed in Figure 2(b). Above 100°C this peak decays and the sample remains essentially amorphous until ~220°C where an intermediate phase forms. This intermediate is characterized by a broad peak just above 5° 2θ and appears to grow in concentration up to 320°C. This intermediate phase then decays just prior to the formation of VO_2 at ~360°C. At 360°C, crystalline VO_2 is first detected, but not as VO2 (T). Instead, one first observes a metastable monoclinic form of VO_2 referred to as VO_2 (B). This has also been observed by Yamamoto, *et al.*, (2009) during the synthesis of VO_2 (T).

They observed that VO_2 (B) typically precedes the formation of VO_2 (T). Hence, the observation of VO_2 (B) serves as a bellwether for imminent VO_2 (T) formation. The structure of VO_2 (B) is detailed by Oka, *et al.*, (1993).

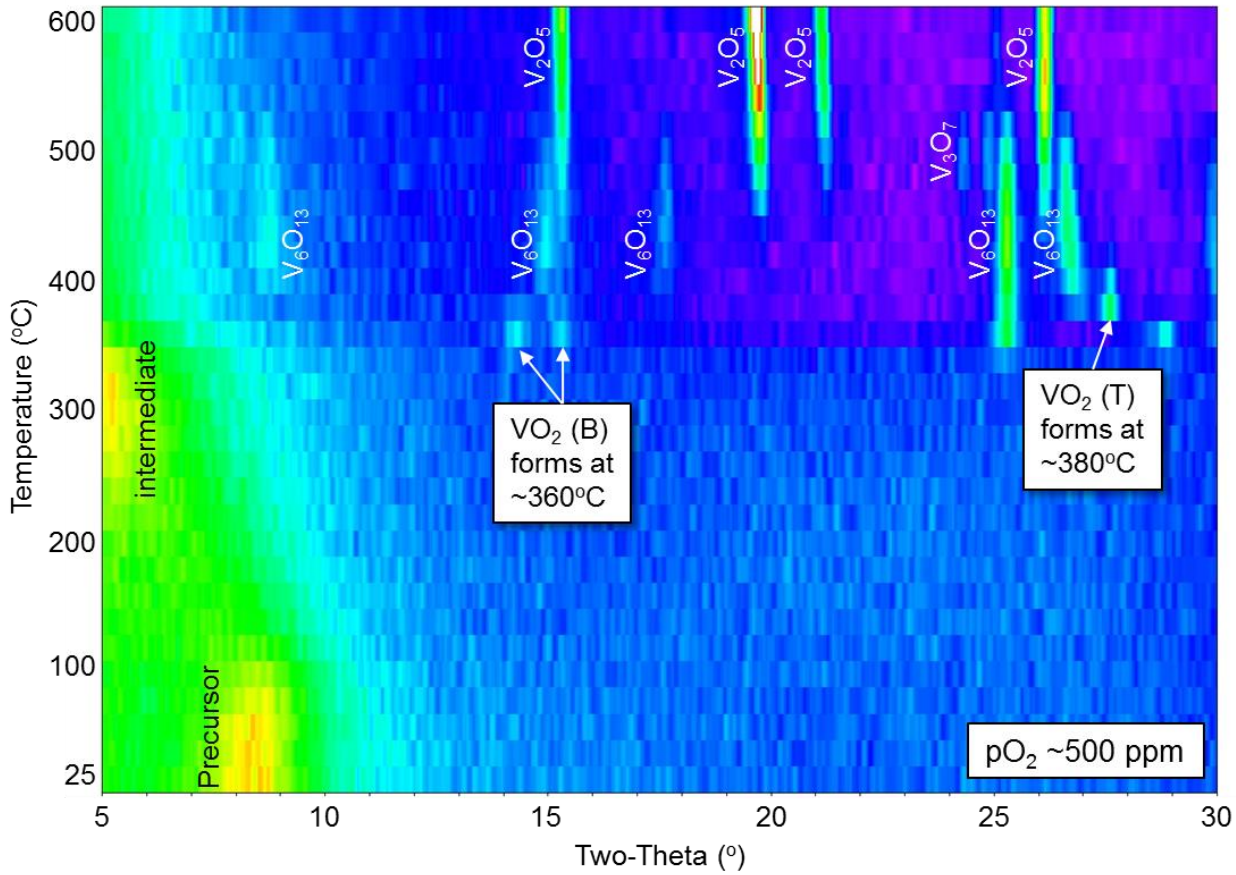

Figure 4. Rainbow contour plot for in-situ heat treatment of VOP powder up to 600°C under a flowing mixture of N_2/O_2 gas (~500 ppm O_2). Intensity is shown as a color scale were purple = low counts, red = high counts. See text for details.

Figure 4 shows that further heating to 380°C yields formation of VO_2 (T); this is characterized by the peak at ~27.6° 2θ which indexes to the (110) of the VO_2 (T) phase. This observation is promising, because it confirms that VO_2 (T) can be formed at low processing temperatures, however, the downside of this result was that the VO_2 (T) was not single-phase. Instead, it coexisted with the V_6O_{13} phase. By 400°C the V_6O_{13} compound was the dominant phase in the step-series. Clearly, the stability range of VO_2 (T) is too small of a processing window for isolation of VO_2 (T) under the oxygen concentration of ~500 ppm. Lowering the pO_2 should aid in expanding the stability range for VO_2 (T) since this would kinetically suppress the reaction-rate through the absence of sufficient oxygen. This shall be demonstrated in the discussion of Figure 5. To complete the discussion of Figure 4, one can see that the V_6O_{13} phase transforms to V_3O_7 at ~480°C, however, there are also signs of V_2O_5 formation as early as 460°C. These three phases coexist up to 500°C and by 520°C only V_2O_5 remains present.

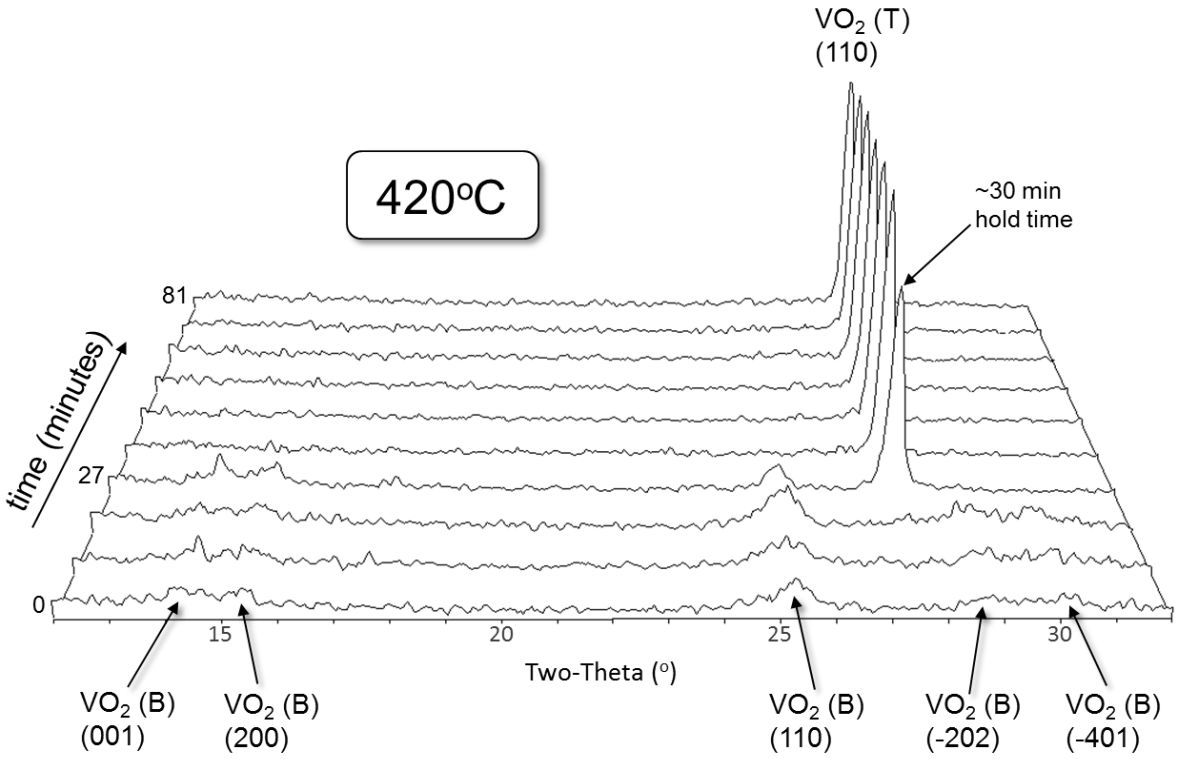

Figure 5. Isothermal hold of VOP precursor at ~50 ppm O_2 at 420°C shows formation of fine grained VO_2 (B) followed by sudden conversion to VO_2 (T) after 30 minutes hold time.

Slowing down the kinetics of phase formation by reduced pO_2 was a successful strategy for isolating VO_2 (T) phase formation. The HTXRD experimental design was changed to the use of isothermal holds at a set pO_2 condition. In this new processing protocol, the sample was heated rapidly (~100°C/min) to the hold temperature followed by immediate and continual collection of XRD scans once the set-point was reached. HTXRD scans employed a shortened 2θ range so as to obtain as much detail about the phase change behavior as possible during the hold time. Typical isothermal hold experiments employed scans that required ~9 minutes to collect, and the duration of the soak time at temperature was ~1.5 hr. This allowed for 10 scans to be collected during this duration. Various pO_2 values and set-point temperatures were attempted. Figure 5 shows the best results for rapid and controlled VO_2 (T) formation. In this isothermal hold experiment, the pO_2 was set to 50 ppm O_2 and the hold temperature was set at 420°C. As the figure illustrates, VO_2 (B) is the only phase observed during the first 3 scans (0-27 minutes). Also notice that the VO_2 (B) peaks are broad, suggesting reduced crystallite size. During the 4th scan in the series we observe decay of the VO_2 (B) phase and dramatic formation of VO_2 (T). Subsequent scans reveal only VO_2 (T) and no additional (higher oxidation state) phases. This result illustrates a simple processing protocol for low-temperature synthesis of VO_2 (T) directly from VOP powder and does not require a multi-step oxidation/reduction procedure. The processing window appears to be wide; the VO_2 (T) phase will form and remain single phase for a significant duration of time (i.e. at least 1 hour as shown in Figure 5).

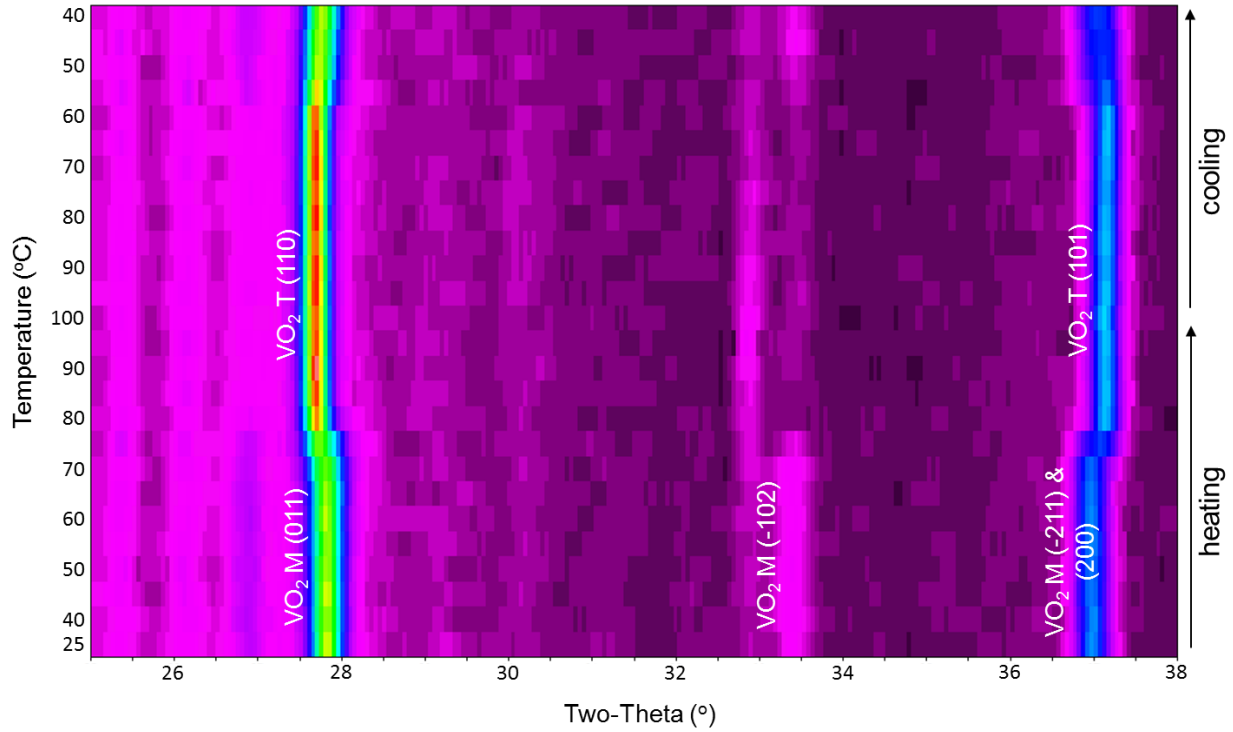

Figure 6. Monoclinic-Tetragonal phase transformation of VO_2 between room temperature and 100°C (air atmosphere). See text for details.

Upon formation of the VO_2 (T) sample documented in Figure 5, the sample was cooled down to room temperature; it showed transformation to the monoclinic form VO_2 (M) as expected. To test the phase transition behavior of the VO_2 between monoclinic and tetragonal, the sample was reheated in an air atmosphere on the hot stage setup (Figure 3) in an attempt to capture the conversion of VO_2 (M) to VO_2 (T). In this step-series experiment the temperature steps were in smaller (5°C) increments to capture the onset of the transition. Figure 6 reveals the outcome of this step-series where the diffracted intensity is plotted as a rainbow scale (purple = low counts, red = high counts). Temperature runs along the y-axis with the initial room temperature scan at the bottom of the plot. During this experiment the temperature was raised up to 100°C during the first 14 XRD scans, labeled as the "heating" portion (see label on right side of figure). Then the sample was cooled back down to ~40°C (labeled as "cooling" on the right of the figure). Both heating and cooling were monitored so as to capture the well-known hysteresis behavior of this transition. Upon heating, the phase transition from the monoclinic VO_2 (M) to the tetragonal form initiated at about 70°C and was complete by 80°C. The transition was easily detected by the sudden shift in the VO_2 (M) (011) peak at ~27.8° 2θ to the VO_2 (T) (110) peak at ~27.6° 2θ. The transition was also captured at ~37.0° 2θ where the superimposed (-211) and (200) peaks of the VO_2 (M) show a shift in 2θ between 70°C and 80°C as the VO_2 (T) (101) peak forms. However, in this case the (101) VO_2 (T) peak is observed at a *higher* angle (~ 37.2° 2θ) than the lower temperature counterparts. The observation of a sudden change in peak location with temperature, coupled with the awareness that these peak shifts occur in opposing angular directions depending on (hkℓ) easily diagnoses this as structural phase transformation behavior (as opposed to thermal expansion or phase decomposition effects). After the maximum temperature of 100°C was reached, the sample was cooled, and the reverse transformation from

VO_2 (T) to VO_2 (M) was observed. In the case of cooling, the transition is delayed until ~60^oC for the onset of the transition and appears to convert back to VO_2 (M) by ~50^oC, although there may continue to be ongoing conversion even in the 50-40^oC range. Hence, we observe a ~10^oC hysteresis between heating and cooling for the monoclinic/tetragonal transition. This is consistent with other reports (e.g. Lu, *et al.*, 2011).

CONCLUSIONS

Low temperature synthesis protocols for conversion of VOP powders to VO_2 (T) have been successfully determined via HTXRD. A straightforward heat treatment of VOP powder under ~50 ppm O_2 at 420^oC reveals initial formation of VO_2 (B) which subsequently converts to VO_2 (T) after ~30 minutes of hold time. Room temperature XRD analysis of the synthesized VO_2 (T) powder shows transformation to the monoclinic VO_2 (M) form. Subsequent temperature cycling through the monoclinic to tetragonal transition reveals the onset of conversion to VO_2 (T) at ~70^oC. Upon cooling, the tetragonal-monoclinic transformation is suppressed by ~10^oC to ~60^oC, illustrating the hysteresis effect of the phase change.

ACKNOWLEDGMENTS

The authors would like to thank Amy Allen (Sandia) for her assistance in the SEM analysis of VOP powders. Sandia is a multiprogram laboratory managed and operated by Sandia Corporation, a wholly owned subsidiary of Lockheed Martin Corporation, for the United States Department of Energy's National Nuclear Security Administration under contract DE-AC04-94AL85000.

REFERENCES

Briggs, R. M., Pryce, I. M., and Atawater, H. A. (2010). "Compact silicon photonic waveguide modulator based on the vanadium dioxide metal-insulator phase transition," *Optics Express* **18** 11192-11201.

Enjalbert, R., and Galy, J. (1986). "A Refinement of the Structure of V_2O_5," *Acta Cryst.* **C42** 1467-1469.

ICDD (2012). PDF4+ 2012 Database, International Centre for Diffraction Data, Newtown Square, PA.

Lazarovits, B., Kim, K., Haule, K., and Kotliar, G. (2010). "Effects of strain on the electronic structure of VO_2," *Phys. Rev. B* **81** 115117-1-9.

Longo, J. M., and Kierkegaard, P. (1970). "A Refinement of the Structure of VO_2," *Acta Chem. Scand.* **24** 420-426.

Lu, Z., Li, C., and Yin, Y. (2011). "Synthesis and thermochromic properties of vanadium dioxide colloidal particles," *J. Mater. Chem.* **21** 14776-14782.

Manning, T. D., Parkin, I. P., Pemble, M. E., Sheel, D., and Vernardou, D. (2004). "Intelligent Window Coatings: Atmospheric Pressure Chemical Vapor Deposition of Tungsten-Doped Vanadium Dioxide," *Chem. Mater.* **16** 744-749.

Oka, Y., Yao, T., Yamamoto, N., Ueda, Y., and Hayashi, A. (1993). "Phase Transition and V^{4+}-V^{4+} Pairing in VO_2(B)," *J. Solid State Chem.* **105** 271-272.

Rogers, K. D. (1993). "An X-ray diffraction study of semiconductor and metallic vanadium dioxide," *Powder Diffr.* **8** 240-244.

Vincent, M. G., Yvon, K., and Ashkenzi, J. (1980). "Electron-Density Studies of Metal-Metal Bonds. II. The Deformation Density of V_2O_3 at 295 K," *Acta Cryst.* **A36** 808-813.

Waltersson, K., Forlund, B., and Wilhelmi, K. A., (1974). "The Crystal Structure of V_3O_7," *Acta Cryst.* **B30** 2644-2652.

Wilhelmi, K. A., Waltersson, K., and Kihlborg, L. (1971). "A Refinement of the Crystal Structure of V_6O_{13}," *Acta Chem. Scand.* **25** 2675-2687.

Yamamoto, S., Kasai, N., and Shimakawa, Y. (2009). "Preparation of Monodisperse and Spherical Rutile VO_2 Fine Particles," *Chem. Mater.* **21** 198–200.

Yang, Z., Ko, C., and Ramanathan, S. (2011). "Oxide Electronics Utilizing Ultrafast Metal-Insulator Transitions," *Annu. Rev. Mater. Res.* **41** 337-367.